21st IMEKO TC4 International Symposium and
19th International Workshop on ADC Modelling and Testing
Understanding the World through Electrical and Electronic Measurement
Budapest, Hungary, September 7-9, 2016

Impedance Spectroscopy: True and Observable Asymptotic Models

Sioma Baltianski [1]

[1] *Wolfson Dept. of Chemical Engineering, Technion – Israel Institute of Technology, Haifa, Israel, cesema@technion.ac.il, Phone +972-4-8292120*

***Abstract* – The decomposition process of the entire impedance spectra into its separate parts is accomplished by data fitting using a parametric distribution function of time constants in a convoluted form. Each particular part of the impedance spectrum is represented as an asymptotic model in the next step. Our technique lies within the branch of direct approaches showed in a concept map that describes analysis options of Impedance Spectroscopy. The direct fitting of the impedance spectrum by a detailed equivalent circuit is challenging due to its ambiguity. A comparative analysis of the asymptotic models is performed using different fitting functions. It is shown here that only Gauss impedance can obtain a "True" asymptotic model. All other known distribution functions used for impedance fitting result in only "Observable" asymptotic model. Correct interpretation relies on obtaining accurate data over wide ranges of frequencies, impedances and temperatures. The results were obtained using a custom-made impedance measurement system based on Precision Impedance Analyser and a Lock in Amplifier. The samples were dense ceramics tested in the temperature range of 200-475 °C and the frequency range of 10^{-2}-3×10^{7} Hz.**

***Keywords* – impedance spectroscopy, asymptotic model, Gauss impedance**

I. INTRODUCTION

The multitude of impedance measurement devices is available on the market. While it becomes relatively easy to collect impedance data, correct analysis or data interpretation are still complicated. The concept map demonstrates main techniques of interpretation of the impedance data [1], Fig. 1. All of these techniques have their advantages and disadvantages.

Here we shall consider only the parametric identification methods. The major shortcoming of the direct electrical model fitting is the ambiguity of the obtained results [2]. A different approach to the interpretation of impedance results is the construction of the distribution function of time constants (DFTC). The core of our approach is the understanding that the DFTC is the primary characteristic that determines the reaction of the object to the electrical stimulus. We believe that this method, in the first step, is more promising than an approach based on the direct electrical model fitting. This is due to the unique distribution function of each tested object.

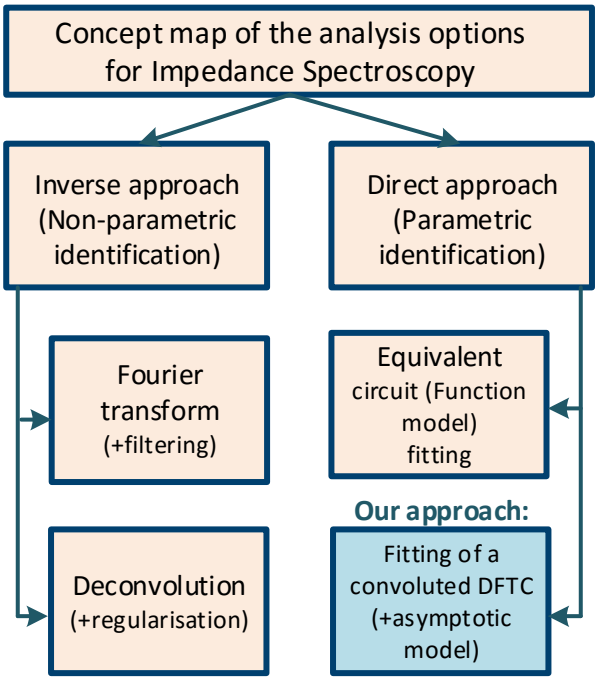

Fig. 1. Concept map of impedance analysis options

The novelty of this paper, especially related to the previous work [2], is studying the non-evident differences in the behaviour of the electric models for different types of time constant distribution. In this work, we analyse the Gauss distribution compared to other types, in particular, ZARC distribution function. In addition, we present a detailed description of the measurement system and its characterization.

II. ASYMPTOTIC MODEL APPROACH

In some cases, the total impedance Z_x can be represented as consecutive independent sections Z_n. Each of the partial impedances is either a process or a constructive feature of the studied object. Barium Titanate ceramic may serve as an example. Its impedance spectra can be separated and associated with the electrode/material interface, bulk and grain boundaries at appropriate temperatures.

Occasionally, it is useful to represent some of the partial impedance Z_n as a cell (lumped elements) and a relaxation core (distributed part), Fig. 2. In particular, the interesting parameters are: C_{cell}, R_{cell}, the total capacity of the relaxation processes $C_{rlx} = \sum_i C_{rlx_i}$ and its time constant.

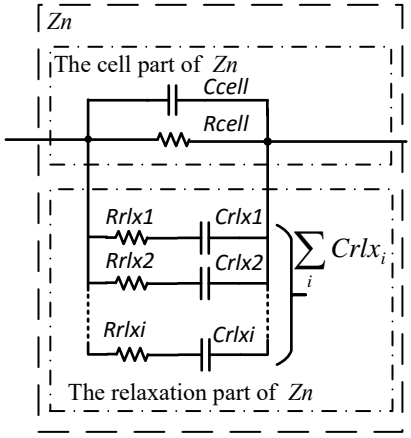

Fig. 2. The cell and relaxation parts of the partial impedance Z_i

Direct fitting of the full impedance spectrum by a sequence of models depicted in Fig. 2 is challenging due to its ambiguity [2]. Another method to parametrically identify the object is constructing the time constants distribution function, which convolution should generate a best possible fit to the experimental data. The distribution function can be composed of a series of peaks [3]. This allows separating the complete DFTC into parametric segments that can be treated independently.

Some of the fitted DFTC parameters are often difficult to link to electrochemical properties or behaviour of the object under examination. An electrical model can help solve this problem. For this purpose, an asymptotic model shown in Fig. 3 has been suggested [4].

The asymptotic values of the cell parameters C_{cell} and R_{cell} are:

$$C_{cell} = -\frac{1}{\omega \operatorname{Im} Z(\omega \to \infty)} \tag{1}$$

$$R_{cell} = \operatorname{Re} Z(\omega \to 0) \tag{2}$$

where: ReZ and ImZ are the real and imaginary parts of impedance respectively and ω is the angular frequency.

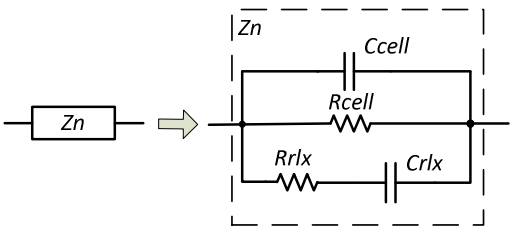

Fig. 3. Asymptotic model

The asymptotic values of the relaxation parameters C_{rlxl} and R_{rlx} are:

$$C_{rlx} = \frac{\operatorname{Im} Y_{rsd}}{\omega(\omega \to 0)} \tag{3}$$

$$R_{rlx} = \frac{1}{\operatorname{Re} Y_{rsd}(\omega \to \infty)} \tag{4}$$

where residual admittance Y_{rsd} is defined as

$$Y_{rsd} = \frac{1}{Z_i} - \left(\frac{1}{R_{cell}} + j\omega C_{cell} \right) \tag{5}$$

III. TRUE AND OBSERVABLE ASYMPTOTIC MODELS

Several fitting functions have been investigated. These functions demonstrate a peak shape in the imaginary part of impedance spectrum and have a peak in DFTC respectively. One of these functions, the Gauss impedance, was described in details in [5]. Additional functions include [6]: ZARC (Cole-Cole), Lorentzian, hyperbolic secant, Warburg, and others. The asymptotic model can be is used to compare different fitting functions.

In this work, we discuss two functions. The first is Gauss impedance (GI). This function describes dipole-dipole interaction (and similar relaxation processes). The second one is ZARC function that describes mass transfer (diffusion and similar processes). Actually, the Constant Phase Element (CPE) determines the distribution of ZARC impedance. The CPE element is explicitly included in the ZARC impedance equation [6]. For a known distribution function of time constants, the corresponding impedance can be obtained by convolution (6).

$$Z(\omega)=\int_0^{\infty} F(\tau)Kz(\omega,\tau)\,d\tau \tag{6}$$

where: $F(\tau)$ – known distribution function, and

$$Kz(\omega,\tau)=\frac{1}{1+j\omega\tau} \tag{7}$$

is the Debye kernel of impedance [6] and ω is an angular frequency.

In the case of a Gaussian distribution we have

$$F_{Gauss}(\tau)=\frac{R_h}{\sigma\sqrt{2\pi}}\exp\left[-\frac{\left(lg(\tau)-\lg(\tau_0)\right)^2}{2\sigma^2}\right] \tag{8}$$

where: R_h – height, σ – standard deviation, τ_0 – characteristic time constant, τ – range of existence in the time domain. Hence, the convolution (6) will give a Gauss impedance.

In the second case, the ZARC distribution function is [7]:

$$F_{ZARC}(\tau)=\frac{R_h}{2\pi}\frac{\sin\left[(1-\alpha)\pi\right]}{\cosh\left[\alpha\ln\left(\frac{\tau}{\tau_0}\right)\right]-\cos\left[(1-\alpha)\pi\right]} \tag{9}$$

here parameter α specifies the distribution, the remaining parameters have the same meaning as above. Consequently, the convolution (6) generates ZARC impedance.

Fig. 4 shows the similarity between the images of the GI and ZARC impedance when using parameters as depicted in the figure.

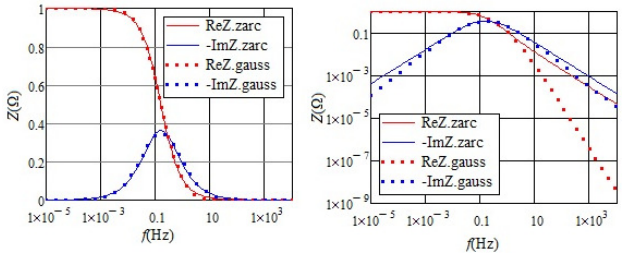

Fig. 4. Comparison of GI (Rh=1, σ=0.5, τ0=1) and ZARC impedance (Rh=1, α=0.8, τ0=1), (a) linear scale and (b) log scale

Despite the similarity of the impedance functions (mainly in the linear scale), the resulting parameters of the asymptotic model are quite different, Fig. 5. This occurs due to different behaviour of the impedance far from the characteristic time constant. Fig. 5 shows the trend of the asymptotic model parameters as a function of the observed frequency range for GI and ZARC impedance and parameters as listed in Fig.4.

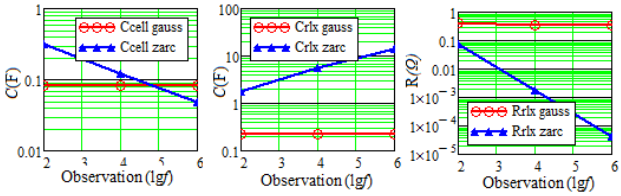

Fig. 5. Comparison of the asymptotic parameters of GI and ZARC impedance as function of the observed frequency range

The values of the cell resistance R_{cell} in both cases remain unchanged and equal (not depicted in the figure). In contrast to the GI, the remaining parameters of the ZARC impedance (C_{cell}, R_{rlx} and C_{rlx},) vary significantly with the observed frequency range. The asymptotic model of Gauss impedance is, therefore, referred to as "True" and ZARC impedance is referred to as "Observable".

In addition, the estimation of the asymptotic models for GI and ZARC impedance was carried out in a wide frequency range (18 orders of magnitude) with increasing approximation order using the model shown in Fig. 2 and LEVM/LEVMW CNLS fitting program [6], Fig. 6. While the parameters of the asymptotic model for GI have stabilized since the third order of approximation (3-RC chains, 6 free parameters), for ZARC all parameters (except R_{cell}) varied monotonically up to the 13th order of approximation (26 free parameters). Thus, the parameters of ZARC asymptotic model (named observable) can be obtained by extrapolation in this case.

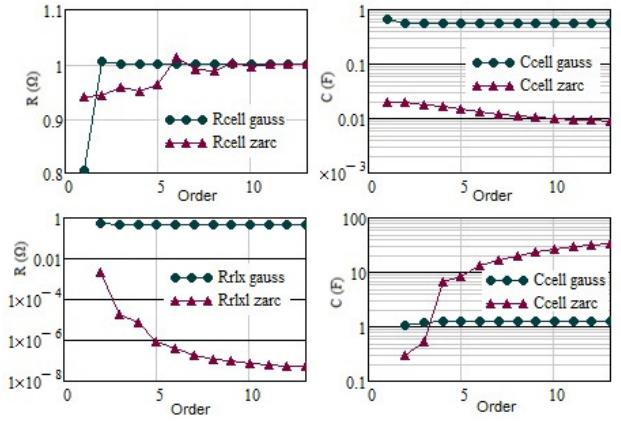

Fig. 6. Comparison of the asymptotic parameters of GI and ZARC impedance as a function of the approximation order

Table 1 shows the parameters of the asymptotic models for GI and ZARC impedance with the parameters shown in Fig. 4.

Table 1. Comparison of the parameters of the asymptotic models for GI and ZARC impedance corresponding to Fig. 4.

Parameters	Gauss distribution Rh=1, σ=0.5, τ_0=1	ZARC distribution Rh=1, α=0.8, τ_0=1
R_{cell}, Ω	1	1
C_{cell}, F	0.557	9.141E-3
R_{rlx}, Ω	0.449	5.251E-8
C_{rlx}, F	1.239	33.493

IV. EXPERIMENTAL

The above discussion generates specific challenging demands for the measuring instruments. Impedance measurements were performed on ceramic samples of Barium Titanate (BT). The electrodes were applied using a commercial Pt paste. The electrical measurements were performed on dense ceramic disks with approximate dimensions of 9.8 mm in diameter and 1.2 mm thick. The homemade sample holder provides a reliable contact in the entire temperature range of the experiment.

A. Measurement System

The system is shown schematically in Fig. 7. Two sufficiently accurate measuring devices provide the main facilities. The first is the Precision Impedance Analyzer (Agilent 4294A, Agilent Technologies) for the high-frequency region. The second is the DSP Lock-in Amplifier (SR 830, Stanford Research System) for the field of low frequencies. Source-meter (Keithley 2400) was used for some DC measurements: for checking of a consistency of the low-frequency measurement, I-V characterization and measurement of the open circuit voltage. Switch/Control System (Agilent 3499A) implements switching from one device to another. The frequency switching point is 100 Hz. The overlapping frequencies are establishing from 100 to 40 Hz and are utilized for adjusting the data by taking into account the calibration files.

In practice, parasitic effects restrict the frequency range of Agilent 4294A from the nominal maximum frequency of 110 MHz to about 30 MHz. This occurs due to the extended path from the end of standard test leads (Agilent 16048G) to the sample under test (SUT) (through the Switch/Control system, the test fixture (Agilent 16034E) and the sample holder). The range of low frequencies is determined by SR 830 and is limited to 1 mHz. Finally, the measuring frequency range was 31.63 MHz-10 mHz with 10 points per decade in uniform logarithmic scale.

Preliminary temperature investigation has shown the reduction of BT impedance value by a magnitude of approximately six orders from room temperature up to 500°C. Therefore, the scheme of a voltage divider has been used to expand the measuring abilities of the Lock-in Amplifier. This scheme is based on the standard resistor of 100 Ω (Agilent 4294-61001) that is actuated by Switch/Control system. The Lock-in Amplifier works in two modes: current measurement at the impedance of $|Z| \geq 0.5$ MΩ and voltage measurement at lower values of impedance.

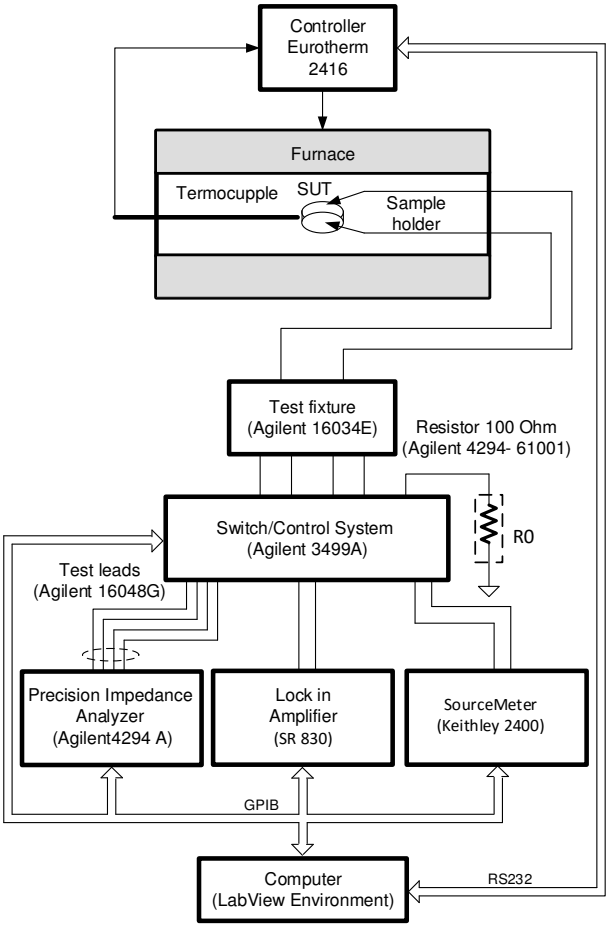

Fig. 7. Measurement system

Measurement circuits for these two cases are shown in Fig. 8. The first circuit (a) is used for high impedance measurement and the second one (b) for low impedance measurement. Known parameters make it possible to get accurate measurement results.

A thermocouple and controller Eroutherm 2416 were utilized to control and measure the SUT temperature. The thermocouple (Type K) is located closely to the SUT inside the furnace. A thermal stability of ± 0.3 ºC at the level of the steady-state regime is ensured.

Operating program (implemented in the LabVIEW environment) provides automatic measuring procedure including primary data processing.

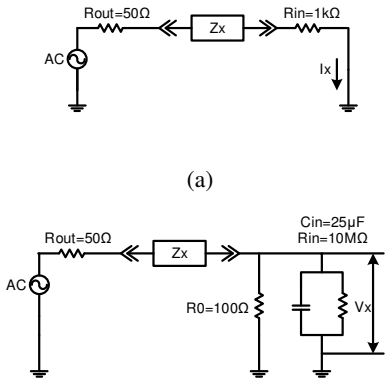

Fig.8. The equivalent circuits for two measurement modes of SR830 Lock-in-Amplifier: (a) current mode, (b) voltage mode

B. System Characterisation

The impedance spectroscopy experiment has been divided into two parts. The first part was based on the physical model (PM). The goal was to estimate the accuracy of the equipment in the operating modes corresponding to real conditions. The physical model is shown in Fig.9. PM was designed using standard lumped elements: resistors and capacitors. The second part was the measurement of the BT sample.

The PM should reproduce a dynamic range of impedance spectrum of the real SUT in a full range of frequencies and temperatures. Moreover, the PM connections to the measurement system should be similar to that of real samples and should be in the same physical environment. This model simulates three areas of impedance spectrum visible in experiments with real samples: electrodes, grain boundaries (GB) and bulk. Influence of temperature was simulated by simultaneous parallel connection of resistors for three temperature modes: "Low T", "Middle T" and "High T". Connections are made by soldering crosspieces for minimization of size and parasitic parameters. The construction is shaped in a cubic form with planar electrodes. The PM is connected to the sample holder inside the furnace.

The *R* and *C* parameters were measured using independent instrument - Precision *LCR* meter (Agilent 4284A). The results are summarized in Table 2. The values were measured within error ± 0.1% according to the specification of Agilent 4284A.

Table 2. Measured values of PM components shown in Fig. 9

Place	*C*, nF	*R1*, kΩ	*R2*, kΩ	*R3*, kΩ
“Electrodes”	2009	1201	129.9	12.00
“GB”	32.41	1479	147.9	14.94
“Bulk”	0.3304	1490	152.1	14.78

Two data sets for each temperature mode of PM are shown in Fig. 10 (there are no visible differences between the sets). The experimental conditions: the temperature of the PM inside the furnace was 30 C°± 0.3 ºC, and the level of the test-signal was 0.5 Vrms.

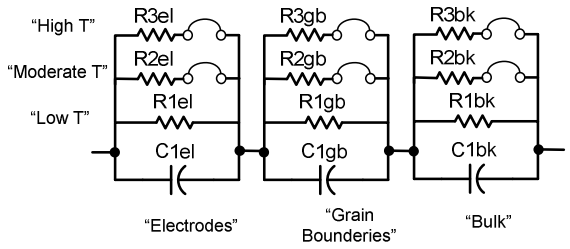

Fig.9. Physical model based on lumped electrical components

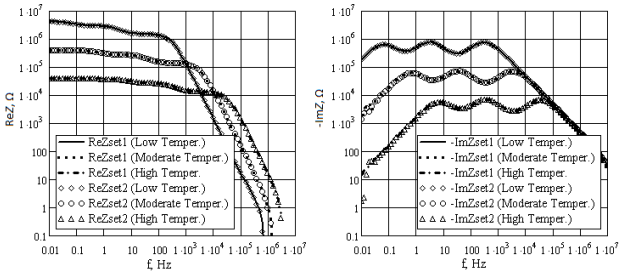

(a) (b)

Fig.10. Two experimental sets of PM impedance for each temperature mode of PM: (a) real part, (b) imaginary part

The instrumental part of errors was estimated by fitting of the equivalent circuit according to PM by using LEVM/LEVMW CNLS fitting program. Relative errors are presented in Table 3.

Table 3. The error of PM parameters found after fitting

Place	δC, %	$\delta R1$, % "Low T"	$\delta R2$, % "Mod. T"	$\delta R3$, % "High T"
“Electrodes”	1.29	-0.62	1.76	0.42
“GB”	-0.14	-0.39	-0.04	-0.01
“Bulk”	-0.26	-0.60	-0.41	-0.01

C. Experiment with $BaTiO_3$ sample

Fig. 11 presents raw data for one of the investigated samples. Two consequent sets of data (~50 minutes each) were recorded at appropriate temperature after 1-hour delay to ensure a steady-state condition. The full experiment takes about 36 hours.

Optimal fitting was obtained using two Gaussians, one of which (low-frequency range) is associated with the grain boundaries and the second one (high-frequency range) with the bulk. Electrode processes were not identified due to the low-frequency range limits. The fitting program was implemented in LabVIEW environment using the Global Optimization function based on a differential evolution method. Arrhenius plots and activation energy (for cell and relaxation parts) were found independently for bulk and grain boundaries, see Fig 12.

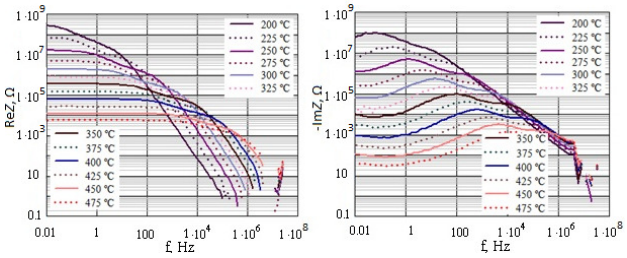

(a) (b)

Fig. 11. Experimental data of BaTiO3 sample: (a) real part, (b) imaginary part

Analysis of the raw data shows an essential distortion in the frequency region of 1 MHz and above. The same distortion (but in a smaller form) is observed when dealing with the physical test model, Fig 10. This effect is due to the influence of the signal leads through the entire path of the measurement system and is caused by resonance effects. Length minimization of these leads is limited mainly due to the physical location of the SUT inside the furnace. Thus, the actual upper-frequency range is 1 MHz, for this type of SUT. When measuring samples with alternative impedance parameters, the range may expand up to 30 MHz.

The fitting of the experimental data was carried out using uniform weighting factor. Thus, the "tail" portions of the high-frequency data will not affect the result of the fitting. At the same time, it seems reasonable to trim the obvious distortion portion of the data when using the data proportional weighting factor. Actually, in our treatment, we used trimmed data.

Additional study was performed to estimate the repeatability (utilizing PM) and the reproducibility (utilizing BT sample). It demonstrated that the described measurement system can be reliably used for studying the behavior of ceramics and similar objects.

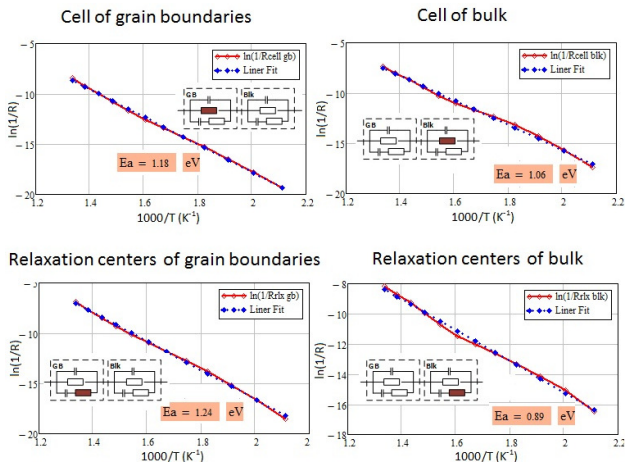

Fig. 12. Arrhenius plots and activation energies

The experimental results demonstrate the possibility to perform studies that are more detailed. For example, one can separately estimate the activation energy of both the cell and the relaxation processes. It is also possible to estimate the density of the relaxation centres (or the dielectric constant) for both the grain boundaries and the bulk.

V. CONCLUSIONS

The analysis of the impedance data is not a straightforward task. Furthermore, high metrological qualities of measuring equipment are required. The direct fitting of the full impedance spectra by a detailed equivalent circuit is challenging due to its ambiguity. Our method is based on the fact that the distribution function of time constants is unique to each object being tested. This method was extended by presenting the results in the form of an asymptotic electrical model.

The concept of "True" and "Observable" asymptotic models was introduced and justified. It has been shown that the model selection should be done with caution when the fitting results are very similar. Selection of the approximation models should take into account the physical aspects and/or other prior information about the object under study.

VI. ACKNOWLEDGMENTS

The author wishes to thank the Center for Absorption in Science and the Ministry of Immigrant Absorption for their support.

REFERENCES

[1]. Tsur, Y., Baltianski, S. "Analyzing Impedance Spectroscopy Results", *Rare Metal Materials and Engineering*, 35 (Suppl.), pp. 452-454, 2006.

[2]. S. Baltianski "Impedance Spectroscopy: Separation and Asymptotic Model Interpetation", *IMEKO World Congress*, pp. 492-497, Prague, Czech Republic, Augst 2006.

[3]. Hershkovitz, S., Baltianski, S., Tsur, Y., "Electrochemical Impedance Analysis of SOFC Cathode Reaction Using Evolutionary Programming", *Fuel Cells*, 12, pp. 77-85, 2012.

[4]. Baltianski, S., Tsur, Y., "Impedance Spectroscopy: Extracting Models", *The Materials Science & Technology. Conference and Exhibition, Pittsburgh*, PA, , pp. 445-452 (Wiley), 2012.

[5]. Baltianski, S., "Impedance Spectroscopy of Electroceramics: The Interpretation Technique", *AES-ATEMA'2014 Eighteen International Conference on Advances and Trends in Engineering Materials and their Applications*. Toronto, Canada, pp. 75-84. August 2014.

[6]. E. Barsoukov, J. R. Macdonald (Eds.), *Impedance Spectroscopy, Theory, Experiment, and Applications*, 2nd Ed., New Jersey, John Wiley & Sons. Inc., 2005.

[7]. J. Macutkevic, J. Banys, A. Matulis. "Determination ofthe Distribution of the Relaxation Times from Dielectric Spectra", *Nonlinear Analysis: Modelling and Control*, Vol. 9, No. 1, pp. 75–84, 2004.